ACS OMEGA

http://pubs.acs.org/journal/acsodf

Article

Solid-State Phosphors from Coal-Derived Carbon Quantum Dots

Anusuya Boruah, Sarmistha Bora, Ashutosh Thakur,* Hemant Sankar Dutta, and Binoy K. Saikia*

Cite This: *ACS Omega* 2023, 8, 25410−25423

Read Online

ACCESS | Metrics & More | Article Recommendations | Supporting Information

ABSTRACT: With unique optical and chemical properties, carbon quantum dots (CQDs) find tremendous applications in chemistry, biology, and materials science to medicine. To expand the applicability of coal-derived CQDs from the liquid to solid state, we herein report the sustainable synthesis of solid phosphors from coal-derived CQDs using poly(vinyl alcohol) (PVA) and silica (SiO_2) as an organic and inorganic matrix. Two coal-derived CQDs were obtained using an eco-friendly ultrasonic-assisted wet oxidation method. The structural and chemical properties of the CQDs were extensively investigated and compared with commercial CQDs. The coal-derived CQDs exhibited blue fluorescence with 8.9 and 14.9% quantum yields. The CQDs were found to be self-co-doped with nitrogen and sulfur heteroatoms through surface and edge functional groups. Solid-state fluorescence of PVA/CQD composite films confirmed that the CQDs retained their excellent blue emission in a dry solid matrix. A facile one-pot sol−gel method was employed to fabricate SiO_2/CQD phosphors with the unique fluorescence emission. Due to their special structural features, coal-derived CQDs favored the heterogeneous nucleation and rapid formation of SiO_2/CQD phosphors. Further, coal-derived CQDs caused high-intensity white light emission with CIE coordinates of (0.312, 0.339) by endowing a suitable band gap structure in a SiO_2/CQD solid phosphor for potential optical applications.

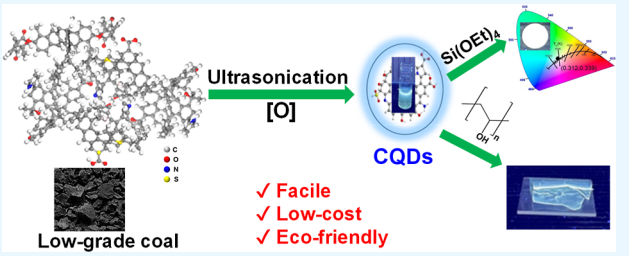

1. INTRODUCTION

Carbon quantum dots (CQDs) are an emerging class of zero-dimensional (0D) crystalline or amorphous nanomaterials of typically ≤10 nm size, and they possess unique optical,[1] physical,[2] and chemical characteristics.[3] Because of their tunable luminescent properties, high chemical/thermal/colloidal stability, low cytotoxicity, good biocompatibility, and biodegradability, CQDs have been widely investigated as potential eco-friendly alternative materials of inorganic semiconductor quantum dots (QDs) for advanced optoelectronic applications such as light-emitting diodes (LEDs),[4] photovoltaic devices,[5] lasers,[6] and photodetectors.[7] Moreover, CQDs are also promising candidates for photocatalysis, energy conversion, bioimaging, biosensing, and drug delivery applications.[2,8−10] Structurally, CQDs are featured with a carbon core and various O/N/S heteroatom functionalities at surfaces and edges. The functional groups act as active sites for potential functionalization, impart high solubility in aqueous solutions, present surface energy traps, and create discrete electronic band structures, thus offering ways to modulate the properties of CQD nanomaterials.[11,12] In recent years, considerable efforts have been put forward on modulating the electronic structure of CQDs by heteroatom doping to improve their performance in various biomedical and optoelectronic applications.[13−16]

The synthesis of CQDs involves either the top-down approach[9,12,17−23] using fairly high-cost starting materials such as graphite, graphene, carbon nanotubes, and photonic crystals, or the bottom-up approach[1,7,18,24−26] using diverse organic molecules (e.g., glucose, ascorbic acid, citric acid, urea, etc.) as building blocks. Although bottom-up approaches offer the feasibility of large-scale CQD synthesis with various structures, the supply chain issue of starting materials of the process may limit the industrial applications of these methods. The recent development of top-down methods for the synthesis of CQDs from the least expensive and abundant coal resources opens up new possibilities for using these nanomaterials in various technologically advanced applications. However, only limited research works have been conducted worldwide on developing carbonaceous nanomaterials from highly abundant coal sources.[27−30] Most notably, our group has developed a novel wet-chemical ultrasonic-assisted, environmentally friendly method for synthesizing bio-compatible heteroatom-doped CQDs and nanodiamonds from highly abundant low-quality Indian coals, coal washery rejects (CWRs), and biomass wastes.[29,31−36] The heteroatom-doped CQDs obtained from coal and biomass sources possess promising fluorescent properties with good quantum efficiency. The fluorescence emission of synthesized CQDs selectively gets quenched in the presence of metal ions, which was exploited to detect silver,

Received: April 27, 2023
Accepted: June 22, 2023
Published: July 6, 2023

mercury, and chromium ions in water.[29,34] Moreover, the metal ion-induced fluorescence quenching of CQDs could be reversible, enabling us to detect fluoride ions in water.[35] Coal-derived CQDs were also used to synthesize silver/CQD nanocomposites that exhibit good antibacterial properties against Gram-positive and Gram-negative bacterial strains.[36] In a recent paper, it has been demonstrated that with proper optimization of the synthesis conditions, the large-scale fabrication of CQDs using inexpensive coal is practically possible.[37]

It is extremely important and interesting to understand the fluorescent properties of our indigenous Indian coal-derived CQDs in solid states for their profitable utilization in new optoelectronic applications. However, these nanomaterials exhibit strong aggregation-induced fluorescence quenching behavior upon drying to the solid state. One way to mitigate this issue is by embedding the CQD nanomaterials in a suitable solid matrix. The solid matrix is expected to provide mechanical strength to the composite material and enhance the chemical stability of CQDs by diminishing their extent of aggregation. In this context, we herein report the synthesis and solid-state fluorescent properties of composite materials of coal-derived CQDs with low-cost silica (SiO_2) as the inorganic matrix and poly(vinyl alcohol) polymer as the organic matrix.

There have been a few reports on the synthesis of CQD-derived solid composites. One study reported the synthesis of solid-state multi-color fluorescent CQDs@SiO_2 phosphors from multi-color CQDs by a reversed-phase microemulsion method.[38] The CQDs@SiO_2 phosphors resulted in the emission of white light under UV irradiation upon mixing at appropriate ratios. In this paper, the reversed-phase microemulsion method for the solidification reaction involved multiple reagents and reaction steps. A similar study reported the synthesis of multi-color emitting SiO_2/CQD composite phosphors by chemically dispersing full-color (blue, green, and red) emitting CQDs on the surface of SiO_2 nanoparticles with the aid of hydrolysis and condensation processes of 3-aminopropyltrimethoxysilane.[39] Another study reported the in situ synthesis of nitrogen-doped CQDs inside SiO_2 particles via pyrolysis of the cation (TMA^+) of tetramethylammonium hydroxide (TMAOH) base employed as a catalyst in SiO_2 particle synthesis.[40] The synthesized composites exhibited tunable fluorescence emission depending on the amounts of TMAOH used in the reactions. In contrast to these processes, our methodology to synthesize SiO_2/CQD composites is facile and simple, involving low-cost coal-derived CQDs and tetraethyl orthosilicate as a SiO_2 precursor. It is important to mention that in our one-pot sol−gel synthesis of SiO_2/CQD composite phosphors, the nature and reactivity of CQDs greatly affect the final composite properties. The results were obtained for two different coal-derived CQD nanomaterials and compared with those obtained for commercial CQDs. Interestingly, the composite of a raw coal-derived CQD nanomaterial with SiO_2 led to single-component white light emission without an additional phosphor with high luminescence intensity when irradiated with UV light. We have thoroughly investigated the CQD nanomaterials using different characterization techniques and tried to demystify the origin of the unique chemical reactivity of coal-derived CQDs and the luminescent properties of their composites with SiO_2.

2. EXPERIMENTAL SECTION

2.1. Materials. All commercially available reagents were of research grade and used without additional purification. Poly(vinyl alcohol) (PVA, 98% hydrolyzed, M_w = 125,000) was purchased from SD Fine-Chem Ltd., India. Commercial carbon quantum dots (C-CQDs, quantum efficiency ≥5%) aqueous solution, tetraethyl orthosilicate (TEOS, 98%) were purchased from Sigma-Aldrich, India. Ethylene diamine (EDA, >98%) was obtained from TCI, India. Ammonium hydroxide (NH_4OH) solution (25%) was used for neutralizing the coal samples after exfoliating them with analytical grade hydrogen peroxide (H_2O_2, 30%, Merck). A low-grade subbituminous Cenozoic coal sample was obtained from the North-eastern coalfield of India. The raw coal sample was processed according to ASTM standard methods described elsewhere.[29−31,37] The CWR samples were obtained from CSIR-CIMFR, Dhanbad (Jharkhand, India).

2.2. Synthesis of Coal-Derived CQDs. Two quantum dot materials based on a raw coal (IC-CQDs) and coal washery rejects (WC-CQDs) were fabricated by using a modified ultrasonic-assisted wet chemical oxidation method. The methodology adopted to fabricate CQDs is similar to that described in our previous papers.[29−31,35−37] Briefly, 30 g of either sample (raw coal or coal reject) was dissolved with 300 mL of H_2O_2 (30%) in an ice-cold condition. The reaction solution was then ultrasonically treated with a frequency of 40 kHz for 6 h at room temperature and pressure in an ultrasonicator (Powersonic 520). The resultant oxidized reaction mixture was then neutralized to pH 7 using a 25% NH_4OH solution. The neutral solution was concentrated using a rotary evaporator (RV10; Ika) to produce the appropriate CQD products after being filtered through 20 μm Whatman quantitative filter paper (ashless, Grade 41) and passed through a 1 kDa ultrafiltration unit (KrosFlo TFF system; SYR2-U10-A; Spectrum). The dry weight of the CQD samples was found to be 3 and 10 mg/mL for WC-CQDs and IC-CQDs, respectively.

2.3. Fabrication of PVA/CQD Composite Film. To prepare PVA/CQD films, PVA powder (200 mg) was dissolved in 2 mL of deionized (D.I.) water under magnetic stirring at 80 °C. After that, a CQD aqueous suspension was added to the polymer solution, corresponding to 2 wt % of CQDs in the composite. The final volume of the water in the reaction mixture was fixed at 4 mL. The mixing reaction was performed under magnetic stirring at 80 °C for 8 h. After that, additional bath sonication was performed for 10 min to obtain a good CQD dispersion. The PVA/CQD solution was poured into a glass Petri dish and dried under vacuum at room temperature for several hours. The polymer composite film formation occurred upon water evaporation, and the film was used for solid-state fluorescence investigations. The composite films derived from three different CQD nanomaterials are assigned as PVA/C-CQDs, PVA/WC-CQDs, and PVA/IC-CQDs, respectively, for commercial CQDs, CWRs-based CQDs, and raw coal-based CQDs. A PVA film without CQDs was synthesized using the same procedure for comparison.

2.4. Synthesis of SiO_2/CQD Composites. To synthesize SiO_2/CQD composites, a sol−gel reaction of tetraethyl orthosilicate (TEOS) was performed in the presence of a fixed amount of CQD sample using ethylenediamine (EDA) as the catalyst. For the reaction, 0.9 mL of TEOS was dissolved in 14.7 mL of ethanol under magnetic stirring at 40 °C. To this solution, a CQD aqueous suspension was added, corresponding to 1.5 wt % of CQDs with respect to the mass of TEOS. The reaction solution was adjusted to 19.9 mL volume by using water. After that, 100 μL of EDA was added immediately to initiate the reaction, and the reaction was stirred at 480 rpm for 3 h at 40 °C.

https://doi.org/10.1021/acsomega.3c02884
ACS Omega 2023, 8, 25410−25423

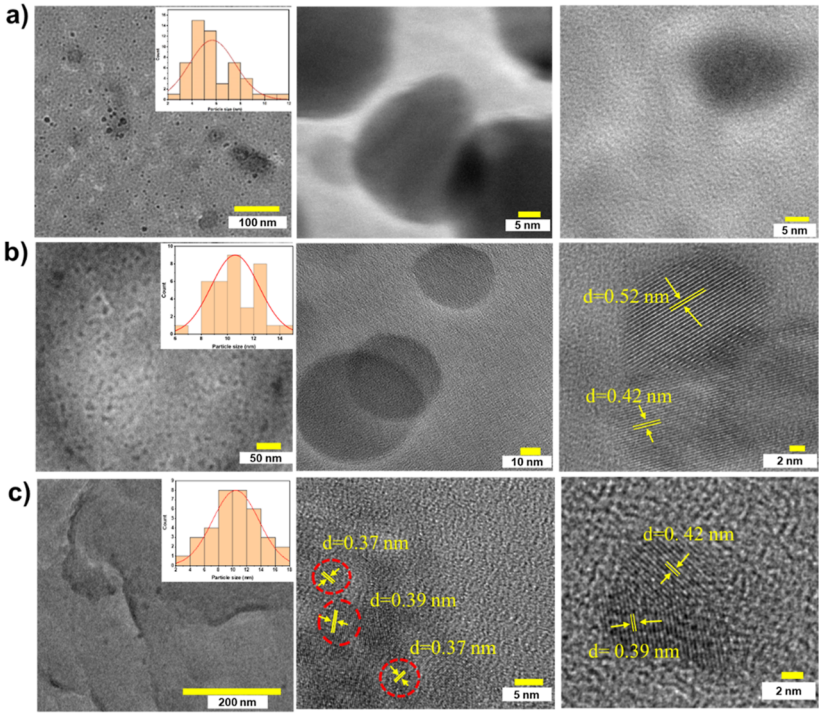

Figure 1. TEM images of the three CQD samples at different magnifications. (a) C-CQDs, (b) WC-CQDs, and (c) IC-CQDs. The insets show size distribution diagrams.

After 3 h, the solid product was separated by centrifugation at 7000 rpm, washed twice with D.I water, and dried in vacuo for 5 h at 70 °C. The composite powder samples derived from three different CQD nanomaterials are assigned as SiO_2/C-CQDs, SiO_2/WC-CQDs, and SiO_2/IC-CQDs, respectively, for commercial CQDs, CWRs-based CQDs, and raw coal-based CQDs. A SiO_2 sample (assigned as N−SiO_2) without CQDs was synthesized using the same procedure for comparison. All solid powder products thus obtained were made into pellets of diameter 1.3 cm at a pressure of 100 tons for solid-state fluorescence investigations.

2.5. Analytical Characterization. The CQD nanomaterials and their solid composites were studied by several characterization techniques. High-resolution transmission electron microscopy (HR-TEM) was used to analyze the nanostructures of the CQDs. HR-TEM images were acquired on a JEM-2100 Plus electron microscope (JEOL Co., Ltd., Japan) operated at 60−200 kV accelerating voltage. The obtained TEM images were analyzed using the ImageJ software program (version: 1.47). A specimen for the TEM analysis was prepared by drop casting a diluted CQD suspension onto carbon-coated copper grids (300 μm) and allowing it to dry in a desiccator at room temperature. The Fourier transform infrared (FTIR) spectra were recorded in the transmission mode on a PerkinElmer System 2000 spectrophotometer to analyze the functional groups in the CQDs and SiO_2/CQDs samples. The samples were prepared by the KBr method, and the spectra were acquired in the range of 400−4000 cm^{-1} with a spectral resolution of 4 cm^{-1}. The surface chemical analyses of the CQDs and the SiO_2/CQD composites were performed based on X-ray photoelectron spectroscopy (XPS). XPS spectra were acquired on a Thermo-Scientific ESCALAB Xi^+ spectrometer (UK) using a monochromatic Al Kα X-ray source (1486.6 eV). The constant analyzer energies were 200 and 50 eV for the survey spectrum and a high-resolution spectrum, respectively. A narrow scan spectrum was recorded with a step increment of 0.05 eV, and at least five scans were accumulated for each element. The binding energies (BE) were calibrated using the C 1s core-level peak at 284.8 eV as the internal reference. Before XPS measurements, the CQD liquid samples were coated as a thin layer on a small glass slide and dried in a hot air oven at 50 °C. The absorption spectra of the liquid CQD samples were recorded on a UV−visible spectrophotometer (UV 1000+, LabIndia). The UV−vis diffuse reflectance spectra of SiO_2/CQDs samples were also recorded on the LabIndia UV 1000+ spectrophotometer in the region 200−800 nm using a $BaSO_4$ plate as the background. Finely ground powder samples were coated on a $BaSO_4$ plate having 100% reflectance. Fluorescence (FL) measurements of the liquid and solid samples were performed on a Fluorolog-3 spectrofluorometer (Horiba, Japan) by applying excitation wavelengths in the range from 260 to 420 nm. All solid-state FL measurements were performed using the front face modality. The relative FL quantum yields of CQDs were evaluated with respect to quinine sulfate in a 0.1 M H_2SO_4 solution. The absolute FL quantum yields of solid phosphors were measured on the Fluorolog-3 spectrofluorometer using an integrating sphere. The particle morphology of SiO_2/CQDs was investigated using a field-emission scanning electron microscope (SIGMA, Carl ZEISS Microscopy, Germany) at an accelerated voltage of 5 kV. A powder sample was attached to a carbon tape and subjected to Au sputtering prior to the FE-SEM analysis.

3. RESULTS AND DISCUSSION

3.1. Characterization of CQDs and Evaluation of Photophysical Properties. The CQD samples derived from coal washery rejects (WC-CQDs) and the raw coal (IC-CQDs), along with the commercial (Sigma-Aldrich) carbon quantum dots (C-CQDs), have been first characterized by transmission electron microscopy (TEM). The TEM images in Figure 1 reveal the presence of well-dispersed spherical-shaped carbon

https://doi.org/10.1021/acsomega.3c02884
ACS Omega 2023, 8, 25410−25423

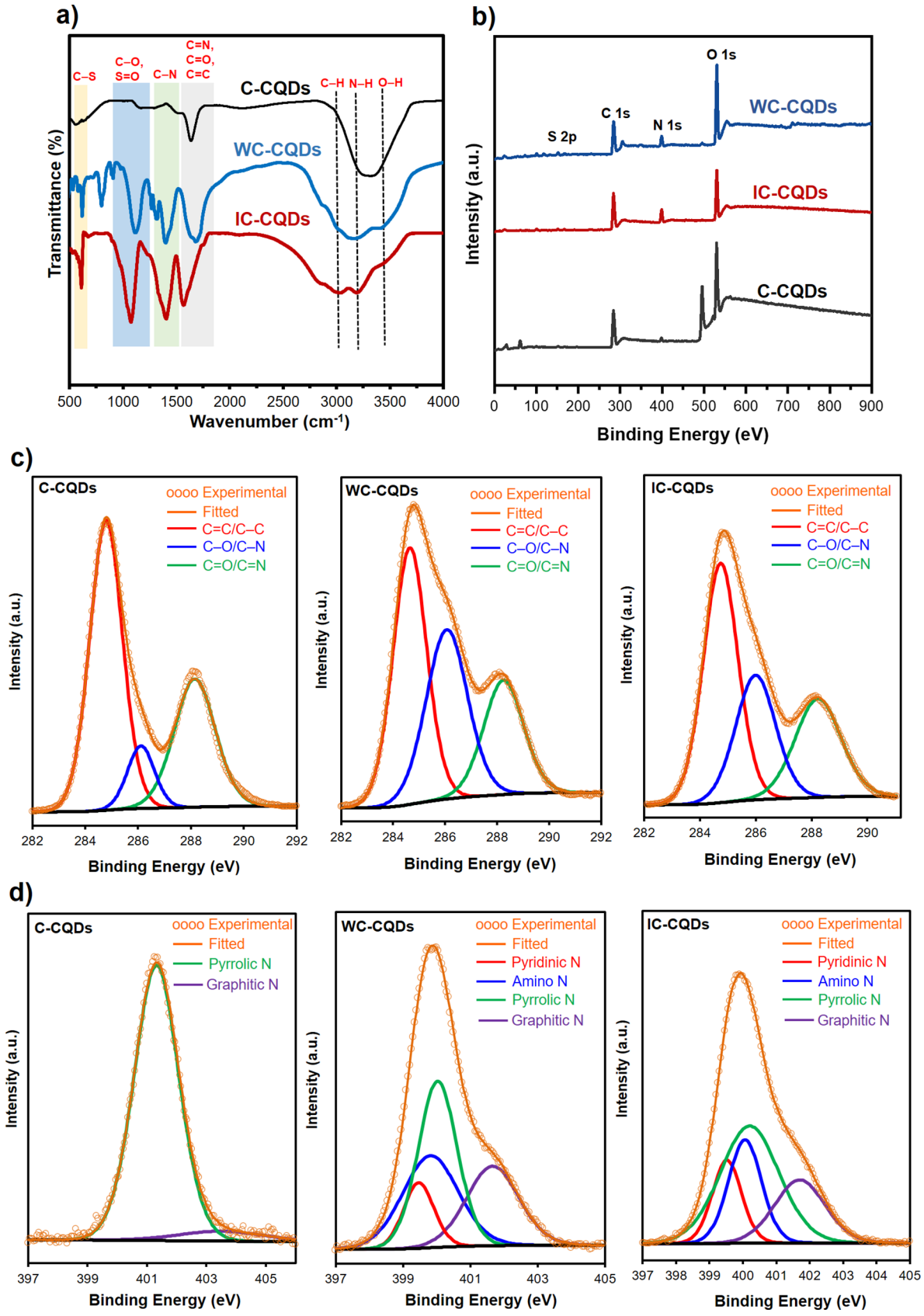

Figure 2. Structural characterization of C-CQDs, WC-CQDs, and IC-CQDs. (a) FTIR spectra, (b) XPS survey spectra, the high-resolution (c) C 1s XPS, and (d) N 1s XPS spectra.

dots with a few agglomerated nanoparticles in all three samples. The statistical average sizes calculated from randomly selected nanoparticles are 5.6 ± 1.8, 10.6 ± 1.8, and 10.4 ± 3.2 nm, respectively, for C-CQDs, WC-CQDs, and IC-CQDs. For better

https://doi.org/10.1021/acsomega.3c02884
ACS Omega 2023, 8, 25410−25423

Scheme 1. Plausible Mechanism for the Formation of CQDs from Sub-bituminous Coal by Oxidative Ultrasonication Method

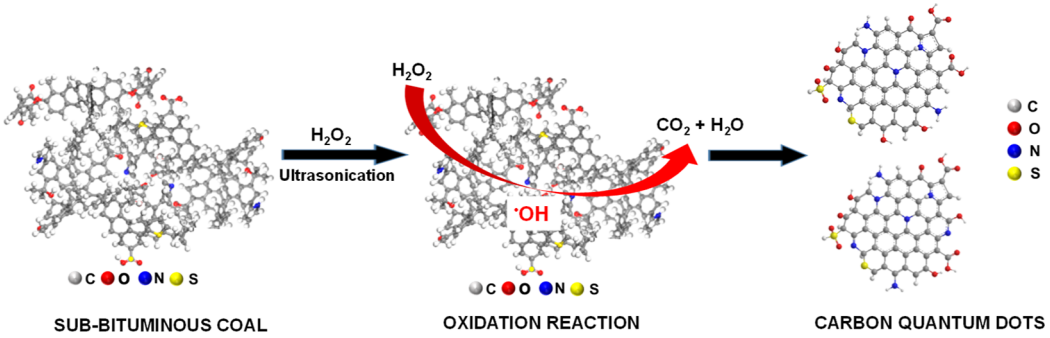

clarity of nanostructures, the high-magnification TEM images of selected nanoparticles with a size similar to or bigger than the average are also presented in Figure 1. Two high-magnification images of different-sized nanoparticles of the commercial sample (Figure 1a) indicate that C-CQD particles are essentially amorphous. On the other hand, the WC-CQDs sample contains both amorphous and crystalline nanoparticles (Figure 1b). The crystalline WC-CQD nanoparticles display well-resolved lattice fringes with *d*-spacings of 0.42 and 0.52 nm, corresponding to the interplanar spacings of heteroatom-doped carbon nanomaterials, as also reported elsewhere.[41] IC-CQD nanoparticles are majorly crystalline (Figure 1c), whose well-resolved lattice fringes with *d*-spacing in the range of 0.37−0.42 nm plausibly correspond to the (002) facets of graphite-like structures. A relatively enlarged *d*-spacing compared to the (002) planes of pure graphitic carbons could be attributed to the presence of lattice defects and/or functional groups in the graphitic planes. So, from TEM analysis, the nanostructures of coal-derived CQDs are found to be uniquely different from those of commercial CQDs.

The chemical structures of three different CQDs, in terms of surface functional groups and elemental composition, have been investigated through Fourier transform infrared (FTIR) spectroscopy and XPS. The FTIR spectra (Figure 2a) show the presence of vibrational bands corresponding to O−H, N−H, C−H, C═C, C═O, C═N, C−N ═, C−O, S═O, and C−S stretching modes of various surface functional groups, such as hydroxyl (−OH), amine/amino ($-NH_2$), carboxyl (−COOH), carbonyl (−CO−), ether (R−O−R), and polyaromatic carbon structures co-doped with O, N, and S elements. The hydrophilic functional groups in CQDs might act as active sites for potential functionalization and impart high solubility to the nanomaterials in aqueous solutions. Among the three samples, IC-CQDs and WC-CQDs display more prominent vibrational bands at 3000, 1410, 1080, and 610 cm^{-1}, respectively, due to the C−H, C−N═, S═O, and C−S stretching modes, suggesting that their polyaromatic structures are more heavily doped with N and S heteroatoms compared with C-CQDs. In addition, the vibrational bands ascribed to N−H and O−H stretching modes at approximately 3200 and 3450 cm^{-1} are rather sharp and discrete for IC-CQDs and WC-CQDs, indicating that the structures of amino ($-NH_2$) and hydroxyl (−OH) groups on the surface of IC-CQD and WC-CQD nanoparticles are different compared with C-CQDs. The XPS survey spectrum (Figure 2b) of all three samples reveals the presence of mainly C, O, and N elements and a small percentage of elemental S. An additional peak at about 500 eV is observed in the survey spectrum of C-CQDs, which can be ascribed to a Na KLL auger signal.[42] The chemical composition of the three CQDs determined using XPS analysis is given in Table S1. It is found that IC-CQDs possess the highest S and N contents of 1.00 and 11.71 at. %, and the S and N contents of the three samples follow this order IC-CQDs > WC-CQDs > C-CQDs (see Table S1). On the other hand, the O content of IC-CQDs (28.28 at. %) is lower than that of C-CQDs (40.59 at. %) and WC-CQDs (41.55 at. %). Taking into account O, N, and S percentages, we conclude that the C content is the highest in IC-CQDs (59.02 at. %) and lowest in WC-CQDs (49.22 at. %) (Table S1). The high-resolution C 1s and N 1s XPS spectra of the three CQD samples are systematically investigated, and the results are presented in Figure 2c,d, and Table S2 (results of peak fitting). The O 1s and S 2p XPS spectra are shown in the Supporting Information (Figure S1). The C 1s spectra of the CQDs are deconvoluted into three peaks centered at about 284.7, 286.1, and 288.1 eV, ascribed to C═C/C−C, C−O/C−N, and C═O/C═N carbons, respectively. Notably, the relative area of the C−O/C−N peak of C-CQDs is much lower than the other C═C/C−C and C═O/C═N peaks, suggesting that C-CQDs possess significantly less hydroxyl and amino groups than carbonyl or carboxyl groups when compared with WC-CQDs and IC-CQDs. This finding is in accordance with the FTIR results and supported by the fact that the O 1s spectrum of C-CQDs can be fitted well by a single C═O peak (other than the peak of H_2O at 535.9 eV). In contrast, WC-CQDs and IC-CQDs show two peaks at about 531.7 and 533.1 eV for organic C═O and organic C−O (Figure S1a). The absence of amino groups in C-CQDs is confirmed by the N 1s spectrum, which shows a rather symmetrical and narrow band mainly composed of pyrrolic N in addition to a small percentage of graphitic N (see Table S2). In contrast, the N 1s spectrum of WC-CQDs and IC-CQDs is composed of four peaks centered at about 399.5, 399.7, 400.0, and 400.6 eV, ascribed to four types of N, namely, pyridinic N, amino N, pyrrolic N, and graphitic N, respectively. The deconvoluted S 2p spectra in Figure S1b show a peak at about 168.5 eV due to S═O for all three CQDs and an additional peak at 163.7 eV in IC-CQDs ascribed to the C−S group.

It should be mentioned that a large number of studies have been reported so far that have judiciously tried to introduce N and S atoms in the structures of CQDs by various chemical reactions. The natural occurrence of N and S in the edge and the carbon lattice makes our coal-derived CQDs unique for many known and unknown applications. A plausible mechanism for the formation of CQDs from sub-bituminous coal has been shown in Scheme 1.[37] Also, as shown in Figure 2c,d and quantitatively reported in Table S2, the relative atomic percentages of different types of C and N atoms are different in the three CQDs, which would dictate the chemical and electronic properties of the nanomaterials. Based on the

https://doi.org/10.1021/acsomega.3c02884
ACS Omega 2023, 8, 25410−25423

characterization results, three models to qualitatively represent the structural differences among the three kinds of CQDs are considered and depicted in Figure S2.

The photophysical properties of the three CQD samples have been investigated by ultraviolet−visible (UV−vis) and fluorescence (FL) spectroscopy. The UV−vis spectra (Figure S3) of aqueous solutions of the CQDs show absorption bands below 250 nm due to the $\pi-\pi^*$ transition of electrons of aromatic π systems. The extension of the absorbance with a tail up to around 350 nm could be attributed to the $n-\pi^*$ electron transition of surface functional groups containing O and N atoms. A fascinating property of CQDs is their visible FL emission in the colloidal solution state. All three types of CQDs in aqueous solutions exhibit bright bluish FL when illuminated with UV light at 365 nm (insets in Figure 3). The special optical property is attributed to discrete electronic band structures of CQDs having conjugated π-domains with various functional groups, quantum confinement effects, and the formation of optically active defect centers. The FL spectra of the CQDs, recorded at different excitation wavelengths ranging from 280−420 nm with an increment of 20 nm, are shown in Figure 3. It is found that all three CQDs exhibit excitation-dependent broad emission characteristics, typical for CQD semiconductor materials having large band gaps. The maximum FL intensity of the three CQDs is observed at 445 nm for IC-CQDs, 442 nm for WC-CQDs, and 428 nm for C-CQDs, respectively, which all correspond to the blue region. As also reported in earlier studies,[43] a slight red shift in the FL emission for the coal-derived CQDs can be correlated with their high N contents. The FL quantum yields (calculated based on the formula shown in eq S1) of the coal-derived WC-CQDs and IC-CQDs are 8.9 and 14.9%, respectively. The higher quantum yield of IC-CQDs could be attributed to higher N and S heteroatom contents, and the result is in accordance with our earlier findings.[37] On increasing the excitation wavelength, the FL spectra of CQDs undergo a continuous red-shift, with the peak maximum reaching up to 500 nm for the excitation wavelength of 420 nm. In addition, with increasing excitation wavelengths, the emission intensity of FL spectra gradually decreases. The excitation-dependent FL is a unique property of colloidal CQDs, which, even though not well understood, could be grossly attributed to the distribution of nanoparticles with varying sizes having different preferential excitation wavelengths, the existence of different fluorophore systems, and emissive traps on nanoparticle surfaces, as confirmed by the FTIR and XPS analyses (Figure 2). The fluorophores of CQDs with aromatic and heteroatom-containing functional groups are selectively excited depending on the wavelength of the light source.

3.2. Solid-State Fluorescence Investigation of PVA/CQD Films. The CQD nanoparticles generally tend to agglomerate, and their colloidal FL emission gets quenched when dried to a solid state.[38] The aggregation-induced luminescence quenching makes it difficult to prepare solid-state CQD phosphors having satisfactory luminescence properties. However, for the profitable utilization of coal-derived CQDs, for instance, in modern optoelectronic applications, it is essential to investigate their solid-state FL properties. After comprehensively evaluating the nature and properties of the CQDs, we next investigated the solid-state FL of PVA/CQD composite films prepared using the identical weight percentage (2 wt %) of the three CQDs. PVA was chosen as a polymer matrix because of its hydrophilic nature and high optical transparency, making it compatible with water-soluble CQDs to

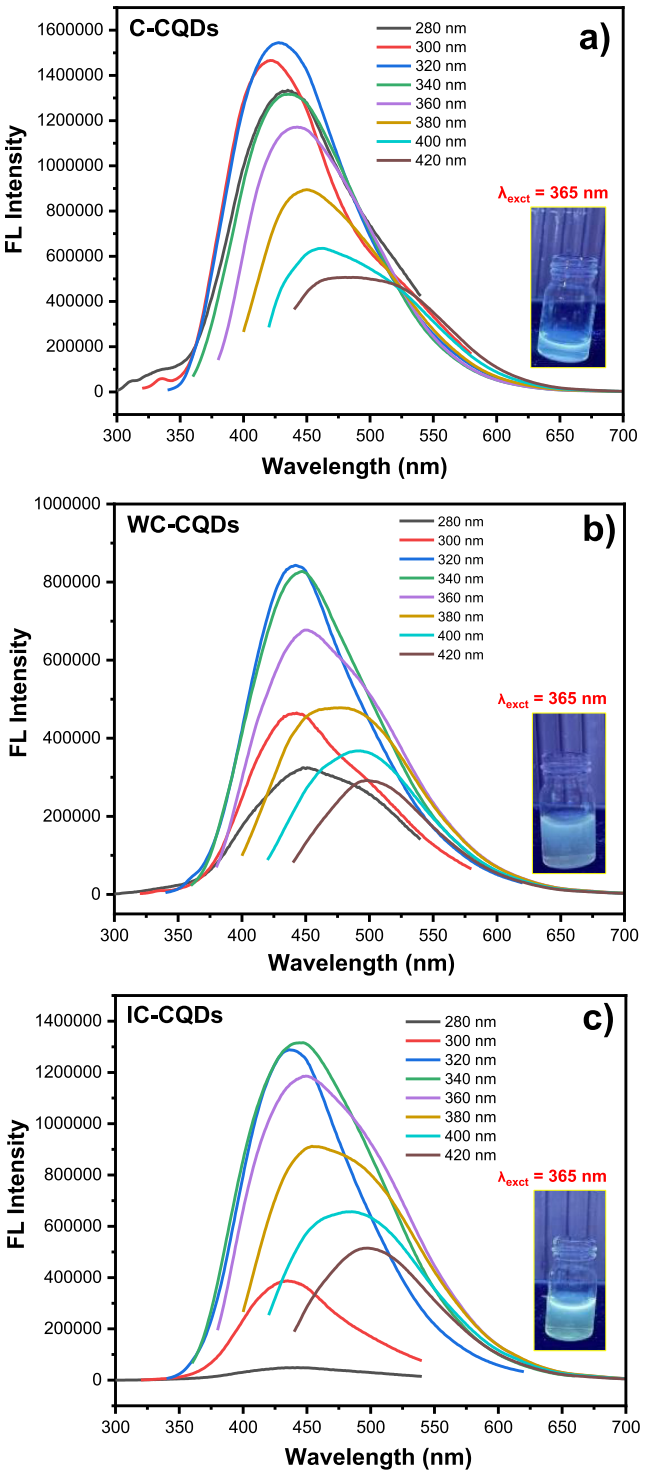

Figure 3. Fluorescence spectra of CQD solutions acquired at different excitation wavelengths. (a) C-CQDs, (b) WC-CQDs, and (c) IC-CQDs. Insets show the photographs taken under 365 nm UV light.

afford transparent and easily processable nanocomposite films. The PVA/CQD films were obtained after properly mixing CQDs (2 wt %) and PVA (98 wt %) in water, casting the mixed solution on the glass substrate, and evaporating the water. It is found that the nanocomposite films are luminescent and emit bright blue FL (Inset pictures, Figure 4) when illuminated with 365 nm UV light. The pristine PVA film prepared without adding CQDs also exhibits blue luminescence under 365 nm UV

https://doi.org/10.1021/acsomega.3c02884
ACS Omega 2023, 8, 25410−25423

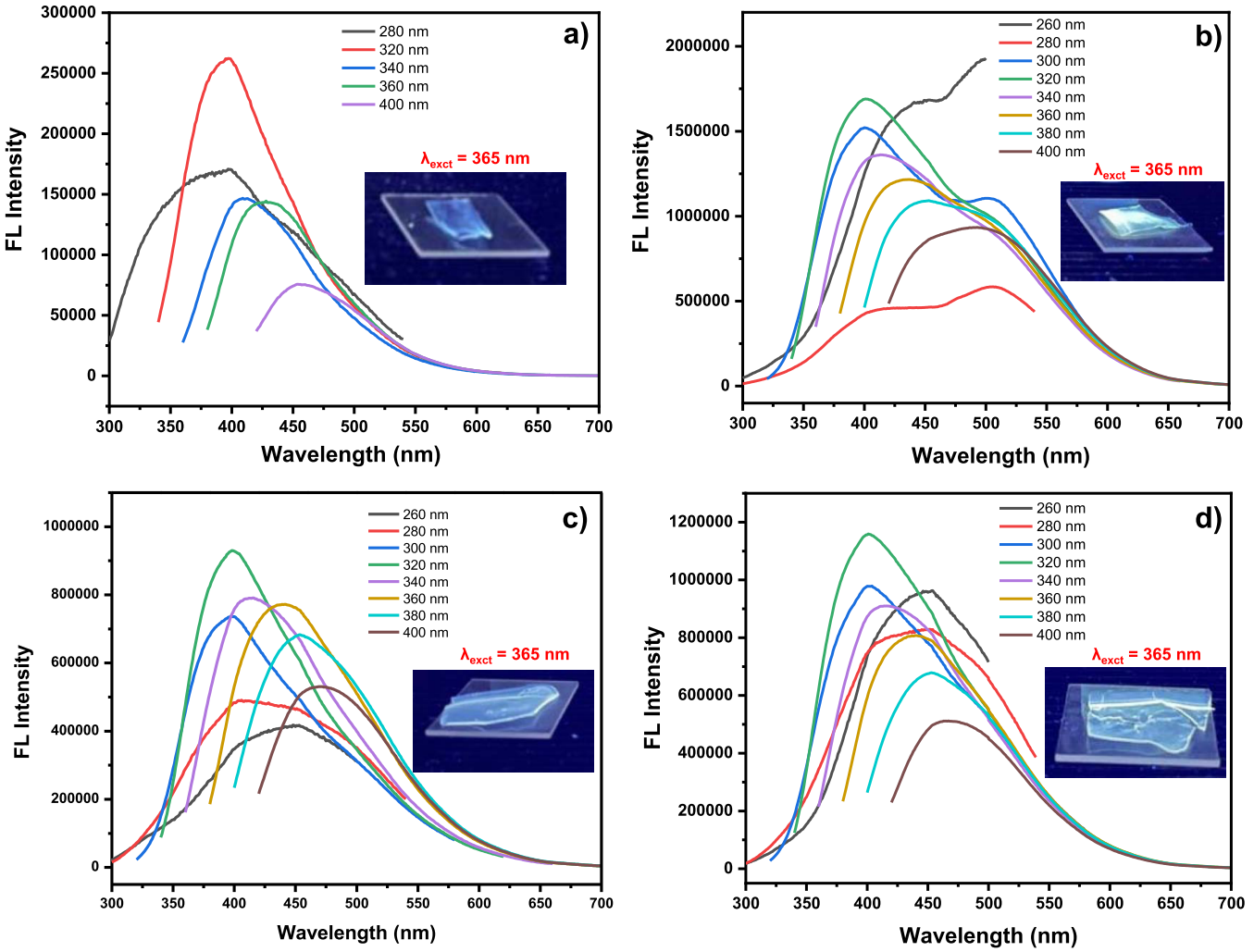

Figure 4. Fluorescence spectra of PVA/CQD composite films acquired at different excitation wavelengths. (a) Pure PVA, (b) PVA/C-CQDs, (c) PVA/WC-CQDs, (d) PVA/IC-CQDs. Insets show the photographs taken under 365 nm UV light.

light but with significantly reduced intensity. The luminescence of the PVA film could be attributed to the presence of abundant hydroxyl groups in the polymer structure. Solid-state FL spectra were recorded at different excitation wavelengths to explore the luminescence properties of the PVA/CQD nanocomposites. The corresponding FL spectra are shown in Figure 4. It is found that the FL intensities of the nanocomposite films at all excitation wavelengths are far higher than those of the pure PVA film, suggesting that the blue luminescence is mainly caused by the CQD nanoparticles embedded in the polymer matrix. All three PVA/CQD nanocomposite films exhibit excitation-dependent broad FL spectra, similar to CQDs in colloidal solution. These results indicate that the aggregation of CQD nanoparticles could be effectively prevented using PVA as the polymer matrix. PVA has abundant hydroxyl groups, which can form a variety of hydrogen bonds with hydroxyl, carboxyl, and amino groups present in CQD surfaces and thus stabilize the nanoparticles against severe aggregation, at least at low nanoparticle loadings. On the other hand, depending on surface functionalities, the said hydrogen bonding interactions likely influence the luminescence properties of CQDs in the solid state: Differently from the solution, the PVA/C-CQD film exhibits rather broad and bimodal FL spectral characteristics up to the excitation wavelength of 340 nm. IC-CQDs solution does not show a detectable FL signal when excited at 280 nm, whereas, in the solid state, PVA/IC-CQD film exhibits appreciable FL emission at the excitation wavelength of 280 nm. Thus, the solid-state FL data suggest that luminescent CQD nanocomposite films can be easily prepared to apply coal-derived CQD nanomaterials in the field of potential optoelectronic materials.

3.3. Solid-State Fluorescence Investigation of SiO_2/CQD Phosphors. In order to synthesize coal-derived CQD-based inorganic phosphors with good emission properties, SiO_2 was chosen as the matrix because of its low toxicity and unique optical properties. Solid-state SiO_2/CQD phosphors were attempted to be prepared by the sol−gel reaction of tetraethyl orthosilicate (TEOS) in the presence of a fixed amount of CQD sample using ethylenediamine (EDA) as the catalyst to accelerate the hydrolysis/condensation of TEOS and the growth of SiO_2 particles (see Experimental Section for details). For a fair comparison, SiO_2 particles were also synthesized without using CQDs. In this reaction, the role of EDA as an organic base is first to catalyze the hydrolysis reaction of TEOS to form $Si(OEt)_{4-n}(OH)_n$ (n being 4 for complete hydrolysis) species as the reaction intermediate, and second to catalyze the condensation of $Si(OEt)_{4-n}(OH)_n$ to form SiO_2 particles by the nucleation and growth processes.[44] The condensation

https://doi.org/10.1021/acsomega.3c02884
ACS Omega 2023, 8, 25410−25423

process is believed to be extremely complicated as it involves multiple hydrolyzed intermediate species. In the present process, the EDA may also participate as the condensation agent due to the availability of amino groups to control the growth of SiO_2 particles. It was observed that in the presence of coal-derived CQDs, particles precipitated instantly as soon as all the reagents were added, while in the presence of C-CQDs and the absence of any CQDs, the precipitation of particles took place rather slowly. Coal-derived CQDs are envisioned to participate efficiently in the reaction to accelerate the formation of SiO_2 particles.

FE-SEM images were acquired for the particles of three different SiO_2/CQD materials and SiO_2 particles prepared without CQDs (hereafter assigned as N−SiO_2). The results are shown in Figure 5. All the samples exhibit nearly spherical

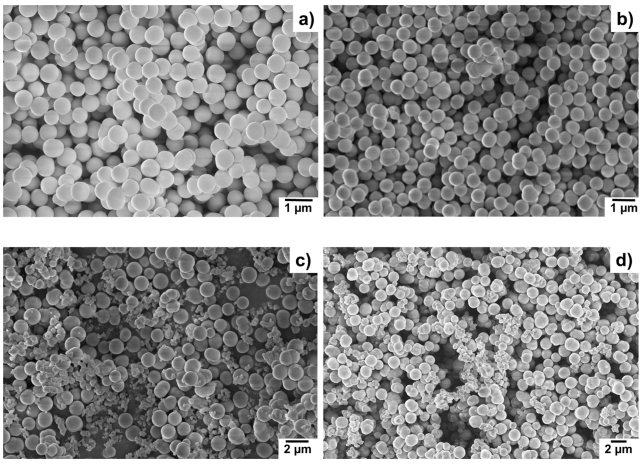

Figure 5. FE-SEM images of (a) N−SiO_2, (b) SiO_2/C-CQDs, (c) SiO_2/WC-CQDs, and (d) SiO_2/IC-CQDs.

particles, while the particle size varies depending on the type of CQD employed. N−SiO_2 and SiO_2/C-CQDs particles are uniform in size and shape, and the particle size ranges between 500 and 800 nm. In contrast, the SiO_2/WC-CQD and SiO_2/IC-CQD samples show the presence of at least two different-sized particles: some particles are large with size ranges between 1 and 1.5 μm, and some are agglomerated small nanoparticles with sizes essentially below 100 nm.

These particle size and shape discrepancies among the four samples support our observation that coal-derived CQDs accelerate the formation of SiO_2 particles and can be explained as follows. As observed from FTIR and XPS spectra (Figure 2), the surfaces of coal-derived CQDs are covered with various functional groups such as carboxyl (−COOH), hydroxyl (−OH), and amino ($-NH_2$). Among these, amino and hydroxyl groups can undergo condensation reactions with hydrolyzed TEOS molecules. Due to their small size (≤10 nm) and crystalline nature (confirmed by TEM in Figure 1), coal-derived CQDs can behave as active centers for the occurrence of heterogeneous nucleation of SiO_2 particles. Because of this phenomenon, the number of nuclei formed dramatically increases in the presence of coal-derived CQD nanoparticles. Consequently, the reaction rate is significantly enhanced, as evident from particle sizes and visual observations. It is known that, in the liquid phase, heterogeneous nucleation occurs faster due to already available stable nucleating surfaces (in this case, coal-derived CQDs), which globally lower the energetic barrier for the nucleation process.[45] However, as the reaction is continued longer in the absence of stabilizing surfactant, the already formed SiO_2/CQD nanoparticles, which are richer in numbers and smaller in size, would undergo coalescence and then Ostwald ripening to form bigger particles, as observed from SEM images. Ostwald ripening is observed for SiO_2 particles under basic conditions,[46] when smaller particles having high surface energy (partially) redissolve in solution and deposit onto larger particles to enlarge particle size. In the absence of CQDs, homogeneous nucleation occurs after multiple condensations of hydrolyzed TEOS precursors. Thus, the formed primary seeds (also called the sol) are smaller in number and would facilitate the growth process at a moderate rate to form uniform particles. The above-mentioned heterogeneous nucleation is less likely to occur with C-CQDs, mainly because of the absence of amino groups and a lower amount of hydroxyl groups on nanoparticle surfaces (Figure 2), as well as the amorphous nature of the nanoparticles (Figure 1). However, we assume that surface functionalities present in C-CQDs are sufficient to make these nanoparticles dispersed in the SiO_2 matrix of SiO_2/C-CQDs either chemically or through hydrogen bonding interactions. The probable mechanism for the formation of SiO_2/CQDs has been provided in Scheme 2.

Given that the maximum theoretical amount of a CQD in a composite is as low as 5 wt % (if all TEOS molecules convert to pure SiO_2) and CQDs are composed of mainly C, O, and N elements (also found in N−SiO_2), it becomes difficult and trivial to detect CQDs in the samples by chemical analysis. XPS has been used to investigate the surface elemental composition; the results are shown in Table S3. All four samples show the presence of Si, O, C, and N elements and a more or less similar elemental composition. Despite a low CQD content in the samples, from deconvoluted C 1s XPS spectra (Figure 6), we can identify the presence of C═O/C═N groups arising from

Scheme 2. Proposed Mechanism Showing the Formation of SiO_2/CQDs

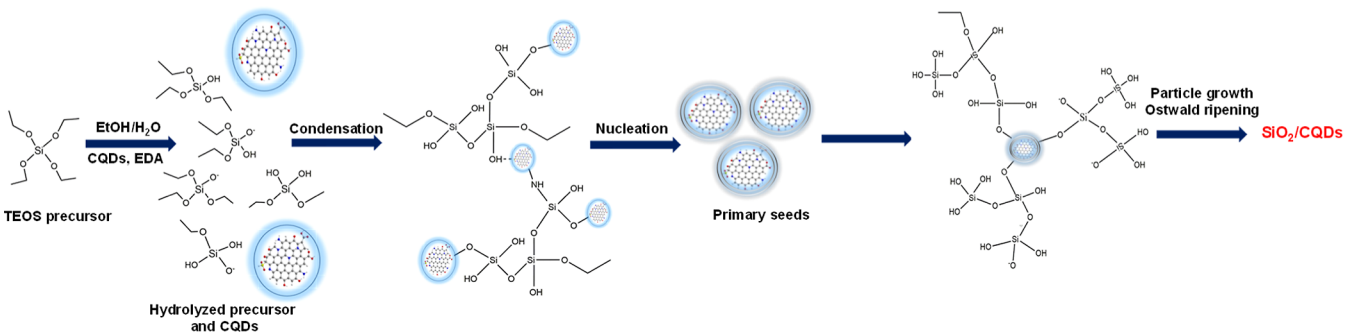

https://doi.org/10.1021/acsomega.3c02884
ACS Omega 2023, 8, 25410−25423

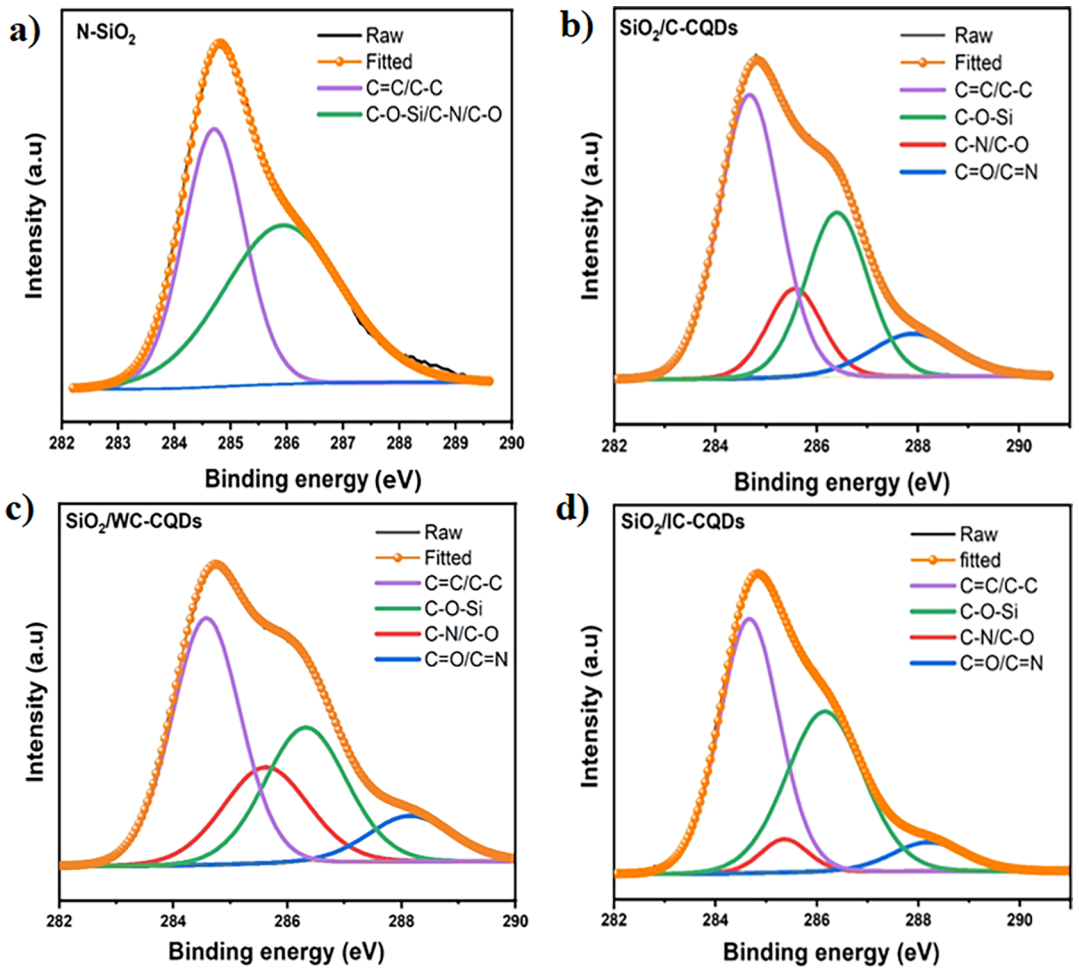

Figure 6. High-resolution C 1s XPS spectra of (a) N−SiO_2, (b) SiO_2/C-CQDs, (c) SiO_2/WC-CQDs, and (d) SiO_2/IC-CQDs.

CQDs in the SiO_2/CQDs samples. FTIR spectra show the presence of vibrational bands at 578, 792, and 1083 cm^{-1} ascribed to Si−O−Si, at 1200 cm^{-1} due to Si−O−C, and at 960 and 1646 cm^{-1} due to Si−OH bonds.[47,48] The broad vibrational band at 1646 cm^{-1} can also be ascribed to C═N, C═O, and C═C stretching vibrations of CQDs present in SiO_2/CQD samples (Figure S4). Moreover, the broadband appearing between 2800 and 3600 cm^{-1} indicates C−H, N−H, and O−H stretching vibrations of various surface functional groups. Medium intensity C−H and N−H bending vibrations are also located at 1460 and 1555 cm^{-1}, respectively.

Next, the optical properties of the synthesized N−SiO_2 and SiO_2/CQDs were investigated by recording the solid-state FL spectra of the samples under various excitation wavelengths ranging from 260 to 420 nm. Samples were prepared as pellets by the hydraulic pressing method and subjected to FL spectroscopic investigation. Interestingly, as shown in Figure 7a, N−SiO_2 exhibits strong FL emission under all excitation wavelengths, and its emission is excitation wavelength-dependent. The maximum emission for N−SiO_2 is observed at 440 nm when the excitation wavelength is 280 nm. The emission intensity gradually decreases, and the peak shape changes with increasing excitation wavelengths. Overall, the FL spectra of N−SiO_2 are broad, unsymmetrical, and deviate from the conventional Gaussian shape. The luminescent properties of N−SiO_2, whose particles are essentially over 500 nm, can be attributed to various surface defect states or optically active defect centers formed due to the incomplete hydrolysis/condensation of TEOS, poor crystallinity of the silica core, and the presence of N-containing functional groups.[49,50] The SiO_2/CQD samples also exhibit excitation wavelength-dependent strong FL emission (Figure 7b−d); however, the FL spectra tend to differ from N−SiO_2 in emission intensity, shape, and broadness. These differences are ascribed to the presence of CQDs as emission centers in the SiO_2 matrix and the change in structural properties brought by CQDs during SiO_2 particle synthesis. Among all the samples, the FL spectra of SiO_2/IC-CQDs appear very broad. The maximum emission intensity of SiO_2/IC-CQDs, when excited at 280 nm, is also the highest among the four samples. The difference in the emission of SiO_2/IC-CQDs is better visualized upon plotting the 360 nm excited FL spectrum of all four samples in Figure 7e. The FL spectra of N−SiO_2, SiO_2/C-CQDs, and SiO_2/WC-CQDs in Figure 7e show the peak maximum below 550 nm and the emission tailed up to 650 nm. In contrast, the spectrum of SiO_2/IC-CQDs extends from 380 nm to over 700 nm, with two distinct emission maxima at 405 and 580 nm, respectively. The spectral power distribution curve of SiO_2/IC-CQDs (Figure S5) at the excited wavelength of 360 nm shows that the FL emission includes all components of the visible spectrum from violet to red light, indicating the emission of white light from SiO_2/IC-CQDs. The luminescent IC-CQDs are assumed to impart unique optical FL properties to the SiO_2/IC-CQD composite by generating photons upon excitation with UV light via the radiative recombination process.

https://doi.org/10.1021/acsomega.3c02884
ACS Omega 2023, 8, 25410−25423

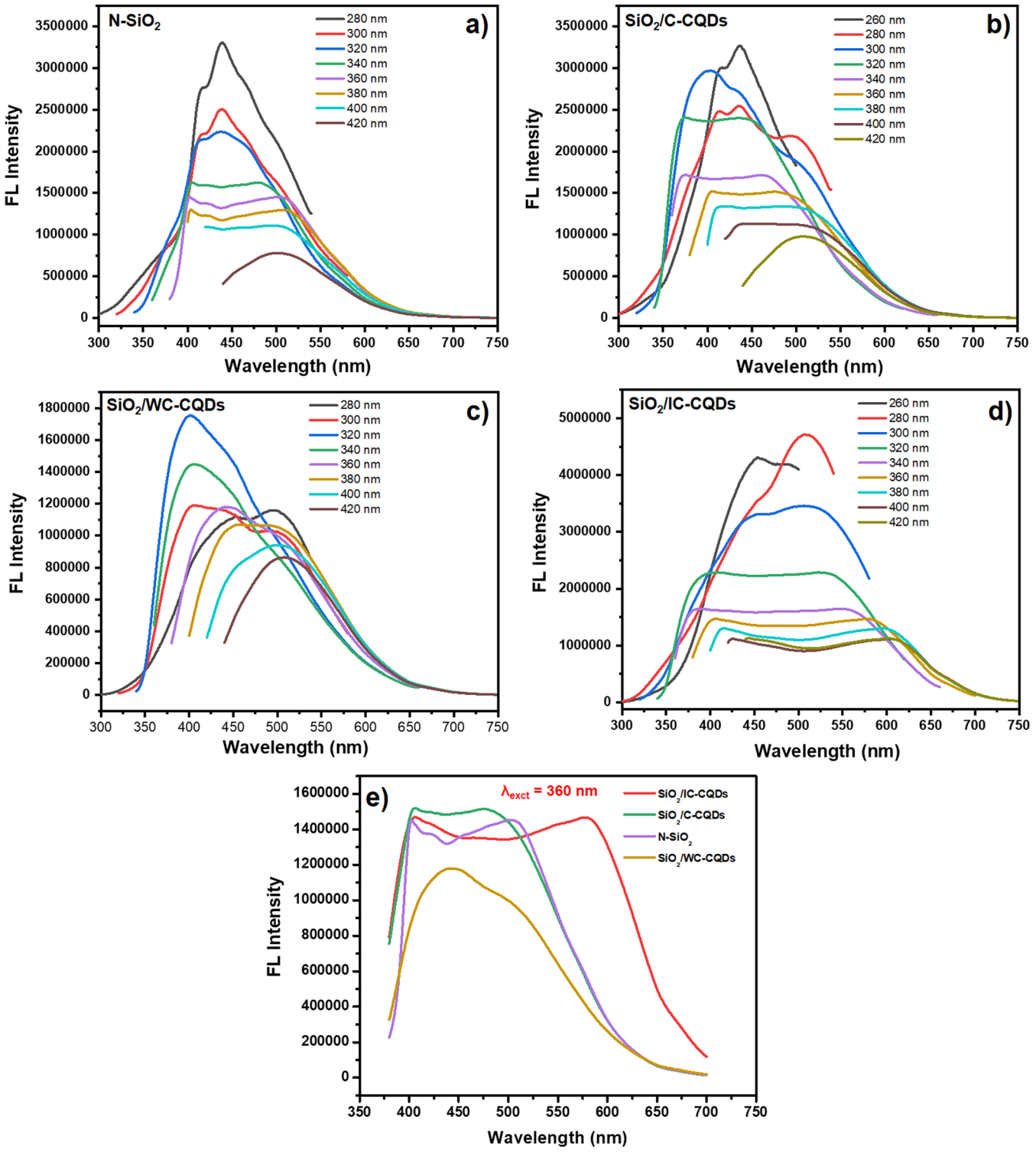

Figure 7. Fluorescence spectra of (a) N−SiO_2 and (b−d) SiO_2/CQD phosphors at different excitation wavelengths. (e) Comparison of fluorescence spectra recorded at the 360 nm excitation wavelength.

The luminescence behavior of N−SiO_2 and SiO_2/CQD phosphors was also recorded by capturing photographs (Figure 8a) of the pellets illuminated under a 365 nm UV lamp. The pellets were placed on glass slides and uniformly exposed to the UV light from the top. It is found that the color of the light emitted from N−SiO_2, SiO_2/C-CQDs, and SiO_2/WC-CQDs appears to be bluish, while the SiO_2/IC-CQDs phosphor emits strong white light covering all parts of the pellet. The Commission Internationale de l'Eclairage (CIE) coordinate plots of the four samples were acquired from the respective 360 nm excited FL spectrum to get more evidence about the color of the emitted light. The CIE coordinates are located (Figure 8b−e) at (0.213, 0.293), (0.209, 0.274), (0.213, 0.265), and (0.312, 0.339) for N−SiO_2, SiO_2/C-CQDs, SiO_2/WC-CQDs, and SiO_2/IC-CQDs, respectively. The (0.312, 0.339) CIE values of SiO_2/IC-CQDs are close to those of pure white light (0.330,

https://doi.org/10.1021/acsomega.3c02884
ACS Omega 2023, 8, 25410−25423

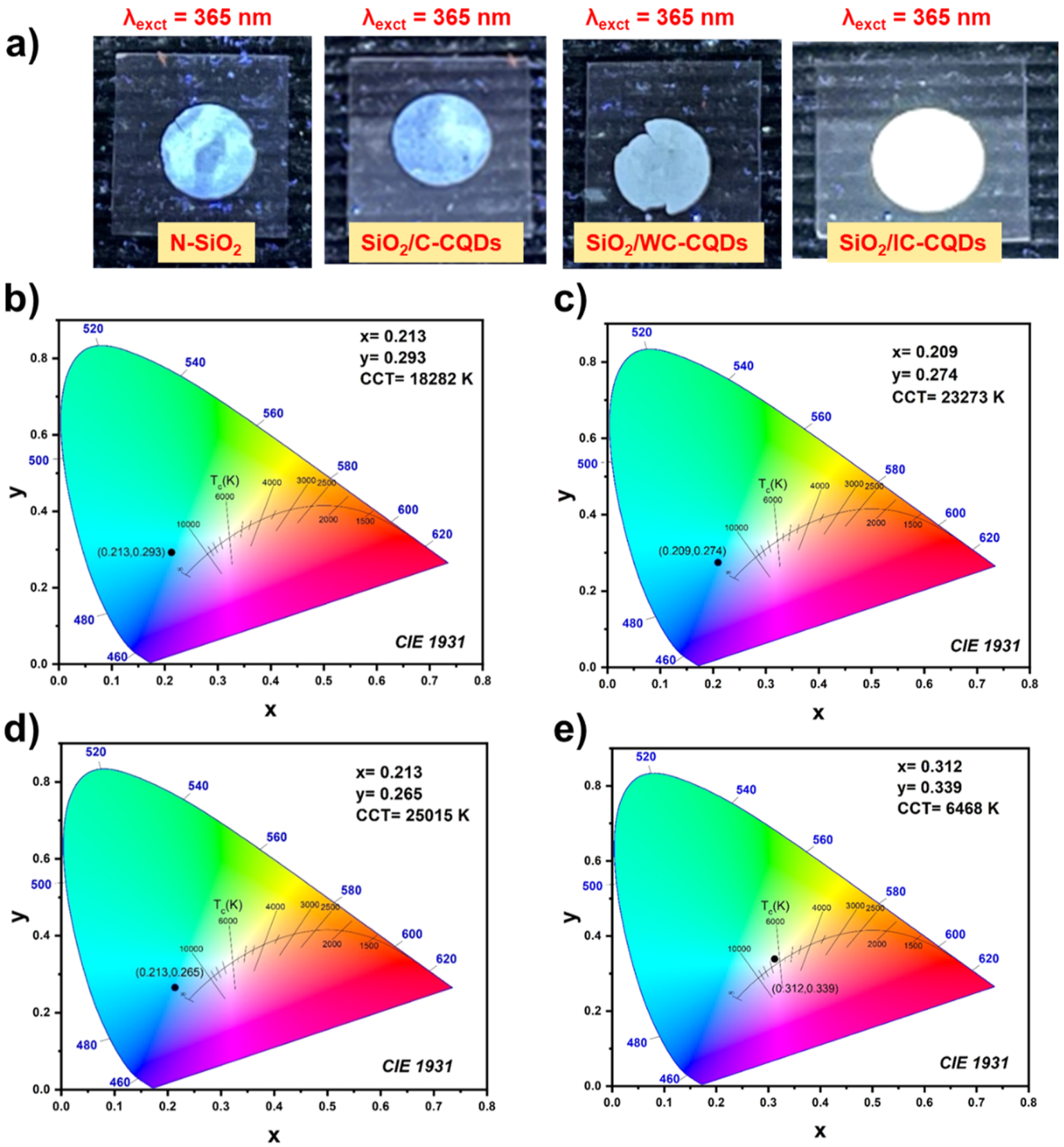

Figure 8. (a) Photographs showing light emission from N−SiO_2 and SiO_2/CQD phosphors under 365 nm UV irradiation. CIE 1931 chromaticity diagrams of (b) N−SiO_2, (c) SiO_2/C-CQDs, (d) SiO_2/WC-CQDs, and (e) SiO_2/IC-CQDs at 360 nm UV irradiation.

0.330). Moreover, the correlated color temperature (CCT) value of the SiO_2/IC-CQD phosphor is calculated to be 6468 K, indicating that the emitted light falls in the cool white light category. Additional experiments were carried out to confirm that the SiO_2/IC-CQD phosphor synthesized at different batches results in similar white light emission (Figure S6) with CIE values of (0.301, 0.342). However, the white light emission is greatly affected when the concentration of IC-CQDs during synthesis increases. The CIE coordinates shift to (0.284, 0.336) and (0.238, 0.298) on increasing the concentration of IC-CQDs by 1.5 and 2.0 times during the synthesis (Figure S6). The FL quantum yield of white-light-emitting SiO_2/IC-CQD phosphor is estimated to be 31.2%, which is higher than that of SiO_2/C-CQDs (26.6%) and N−SiO_2 (23.0%), indicating the positive influence of doping of raw coal-derived IC-CQDs on the luminescent properties of the solid phosphor.

To get more insights into the optical properties of the SiO_2/IC-CQD white-light-emitting phosphor, a solid-state UV−vis diffuse reflectance spectrum was recorded at room temperature. UV−vis DRS spectra of N−SiO_2 and SiO_2/IC-CQDs prepared

https://doi.org/10.1021/acsomega.3c02884
ACS Omega 2023, 8, 25410−25423

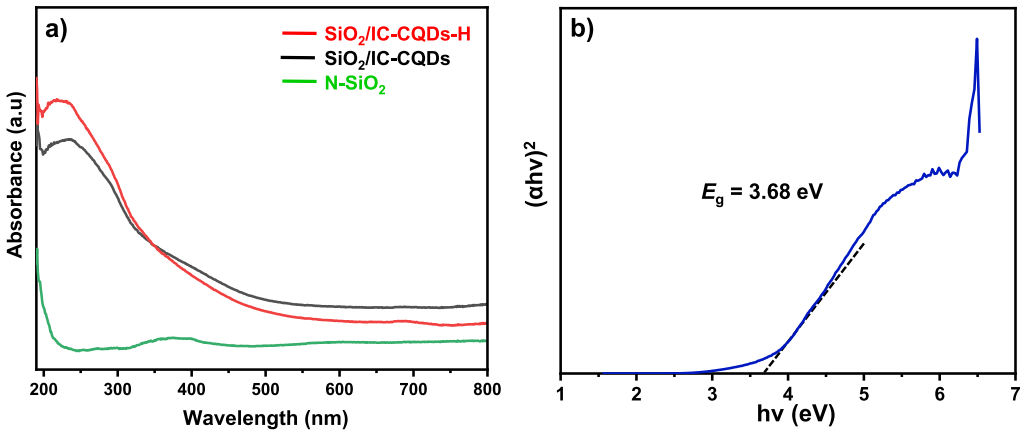

Figure 9. (a) Solid-state UV−vis spectra of N−SiO_2, SiO_2/IC-CQDs white-light-emitting phosphor, and SiO_2/IC-CQDs-H phosphor synthesized using the highest concentration of IC-CQDs. (b) Tauc's plot of the SiO_2/IC-CQD white-light-emitting phosphor.

using the highest concentration of IC-CQDs were also recorded. All the results are shown in Figure 9. The UV−vis absorption spectrum of N−SiO_2 (Figure 9a) indicates that the material has marginal absorbance in the UV region below 210 nm. The absorbance pattern of N−SiO_2 is similar to that of hydrothermally synthesized N-functionalized fluorescent SiO_2 nanoparticles reported elsewhere.[49] SiO_2/IC-CQDs phosphors display strong absorbance at about 230 nm with a noticeable tail up to 550 nm, indicating that some optically active states, different from those in N−SiO_2, are present in these materials. The absorbance value of SiO_2/IC-CQD phosphors increases when the concentration of IC-CQDs is increased during synthesis. These UV−vis results provide ample evidence that the unique absorbance features of SiO_2/IC-CQD phosphors must be associated with coal-derived carbon quantum dots (IC-CQDs) in their structures. Furthermore, the optical band gap (E_g) of the SiO_2/IC-CQD white-light-emitting phosphor is estimated based on Tauc's plot (Figure 9b) for a direct band gap semiconductor. The band gap appears as 3.68 eV, establishing the material as a wide band gap semiconductor having the potential for optoelectronic applications. The presence of a well-defined band gap suggests that the unique FL emission of the SiO_2/IC-CQD white-light-emitting phosphor not only involves defect luminescence but also band gap luminescence.

4. CONCLUSIONS

In conclusion, we have prepared solid-state composite phosphors of indigenous coal-derived CQDs with low-cost and non-toxic PVA and silica (SiO_2) as an organic and inorganic solid matrix. The CQDs retained their blue fluorescence emission in PVA/CQD composite films, broadening the scope of their applications from liquid to solid state. Using a facile one-pot sol−gel synthesis method, we successfully fabricated SiO_2/CQD phosphors with unique fluorescence emission. In contrast to commercial CQDs, coal-derived CQDs significantly accelerated the sol−gel reaction, endowing the rapid formation of SiO_2 particles containing CQDs in their structure. Based on sophisticated structural and chemical analysis, it was confirmed that the small size (≤10 nm) and crystalline nature of coal-derived CQDs, along with their abundant amino and hydroxyl groups, favored the heterogeneous nucleation and rapid formation of SiO_2 particles. Most notably, a SiO_2 composite of a raw coal-derived CQD nanomaterial exhibited broad fluorescence emission spectra with high intensity covering most wavelengths of the visible range. The presence of coal-derived CQDs in SiO_2 particles caused a suitable band gap structure in the composite material, and due to both defect luminescence and band gap luminescence, the material likely exhibited broad white emission characteristics. To our knowledge, this is the first example of the sol−gel synthesis of white-light-emitting solid phosphor from coal-derived CQDs. The results presented here are expected to greatly augment the development of cost-effective solid-state phosphor materials from coal-derived CQDs for their applications in optoelectronic devices as alternatives to conventional inorganic semiconductor materials.

■ ASSOCIATED CONTENT

Supporting Information

The Supporting Information is available free of charge at https://pubs.acs.org/doi/10.1021/acsomega.3c02884.

O 1s and S 2p XPS data of CQDs; elemental analysis of CQDs based on XPS; model structures of CQDs; UV−vis absorption spectra of CQDs; elemental analysis of SiO_2/CQDs based on XPS; FTIR spectra of SiO_2/CQDs; spectral power distribution curve of SiO_2/IC-CQDs; CIE 1931 chromaticity diagrams of SiO_2/IC-CQDs prepared at different batches and using different amounts of IC-CQDs; and equation for estimating fluorescence quantum yield (PDF)

■ AUTHOR INFORMATION

Corresponding Authors

Ashutosh Thakur − *Coal and Energy Division, CSIR-North East Institute of Science and Technology, Jorhat 785006 Assam, India; Academy of Scientific and Innovative Research (AcSIR), Ghaziabad 201002, India;* orcid.org/0000-0002-9089-9560; Email: ashutoshthakur@neist.res.in, thakur.ashutosh13@gmail.com

Binoy K. Saikia − *Coal and Energy Division, CSIR-North East Institute of Science and Technology, Jorhat 785006 Assam, India; Academy of Scientific and Innovative Research (AcSIR), Ghaziabad 201002, India;* orcid.org/0000-0002-3382-6218; Email: bksaikia@neist.res.in, bksaikia@gmail.com

Authors

Anusuya Boruah − *Coal and Energy Division, CSIR-North East Institute of Science and Technology, Jorhat 785006 Assam,*

https://doi.org/10.1021/acsomega.3c02884
ACS Omega 2023, 8, 25410−25423

India; Academy of Scientific and Innovative Research (AcSIR), Ghaziabad 201002, India

Sarmistha Bora − *Coal and Energy Division, CSIR-North East Institute of Science and Technology, Jorhat 785006 Assam, India*

Hemant Sankar Dutta − *Analytical Chemistry Group, Materials Science & Technology Division, CSIR-North East Institute of Science and Technology, Jorhat 785006 Assam, India; Academy of Scientific and Innovative Research (AcSIR), Ghaziabad 201002, India*

Complete contact information is available at: https://pubs.acs.org/10.1021/acsomega.3c02884

Author Contributions

The manuscript was written through contributions of all authors. All authors have given approval to the final version of the manuscript.

Notes

The authors declare no competing financial interest.

■ ACKNOWLEDGMENTS

The authors are thankful to the Director, CSIR-NEIST, for his keen interest in the research field and permission to publish the paper. SAIF, CSIR-NEIST, Jorhat, India, has been thankfully acknowledged for providing instrument facilities. A.T. acknowledges the Science and Engineering Research Board (SERB), New Delhi, for a Start-up Research Grant (SRG/2022/001365). The fund received from CSIR (OLP-2077) is thankfully acknowledged.

■ REFERENCES

(1) Lim, S. Y.; Shen, W.; Gao, Z. Carbon Quantum Dots and Their Applications. *Chem. Soc. Rev.* **2015**, *44*, 362−381.
(2) Rasal, A. S.; Yadav, S.; Yadav, A.; Kashale, A. A.; Manjunatha, S. T.; Altaee, A.; Chang, J. Y. Carbon Quantum Dots for Energy Applications: A Review. *ACS Appl. Nano Mater.* **2021**, *4*, 6515−6541.
(3) Pal, A.; Sk, M. P.; Chattopadhyay, A. Recent Advances in Crystalline Carbon Dots for Superior Application Potential. *Mater. Adv.* **2020**, *1*, 525−553.
(4) Jia, H.; Wang, Z.; Yuan, T.; Yuan, F.; Li, X.; Li, Y.; Tan, Z.; Fan, L.; Yang, S. Electroluminescent Warm White Light-Emitting Diodes Based on Passivation Enabled Bright Red Bandgap Emission Carbon Quantum Dots. *Adv. Sci.* **2019**, *6*, 1900397.
(5) Yuan, T.; Meng, T.; He, P.; Shi, Y.; Li, Y.; Li, X.; Fan, L.; Yang, S. Carbon Quantum Dots: An Emerging Material for Optoelectronic Applications. *J. Mater. Chem. C* **2019**, *7*, 6820−6835.
(6) Liu, L.; Yu, X.; Yi, Z.; Chi, F.; Wang, H.; Yuan, Y.; Li, D.; Xu, K.; Zhang, X. High efficiency solar cells tailored using biomass-converted graded carbon quantum dots. *Nanoscale* **2019**, *11*, 15083−15090.
(7) Huang, J. J.; Zhong, Z. F.; Rong, M. Z.; Zhou, X.; Chen, X.-D.; Zhang, M. Q. An Easy Approach of Preparing Strongly Luminescent Carbon Dots and Their Polymer Based Composites for Enhancing Solar Cell Efficiency. *Carbon* **2014**, *70*, 190−198.
(8) Iravani, S.; Varma, R. S. Green Synthesis, Biomedical and Biotechnological Applications of Carbon and Graphene Quantum Dots. A Review. *Environ. Chem. Lett.* **2020**, *18*, 703−727.
(9) Wang, R.; Lu, K.-Q.; Tang, Z.-R.; Xu, Y.-J. Recent Progress in Carbon Quantum Dots: Synthesis, Properties and Applications in Photocatalysis. *J. Mater. Chem. A* **2017**, *5*, 3717−3734.
(10) Zhu, P.; Li, W.; Zhang, Y.; Sun, Q.; Lin, Y.; Qiu, A.; Chen, X.; Zhou, Y.; Wu, G.; Li, Y.; Yu, Z.; Xu, Q.; Luo, D.; Cai, L. *β*-Cyclodextrin Derived Full-Spectrum Fluorescent Carbon Dots: The Formation Process Investigation and Biological Applications. *Chin. Chem. Lett.* **2023**, 108239.
(11) Wang, Y.; Hu, A. Carbon Quantum Dots: Synthesis, Properties and Applications. *J. Mater. Chem. C* **2014**, *2*, 6921−6939.
(12) Li, L.; Wu, G.; Yang, G.; Peng, J.; Zhao, J.; Zhu, J.-J. Focusing on Luminescent Graphene Quantum Dots: Current Status and Future Perspectives. *Nanoscale* **2013**, *5*, 4015−4039.
(13) Park, Y.; Kim, Y.; Chang, H.; Won, S.; Kim, H.; Kwon, W. Biocompatible Nitrogen-Doped Carbon Dots: Synthesis, Characterization and Application. *J. Mater. Chem. B* **2020**, *8*, 8935−8951.
(14) Liu, L.; Yu, X.; Yi, Z.; Chi, F.; Wang, H.; Yuan, Y.; Li, D.; Xu, K.; Zhang, X. High Efficiency Solar Cells Tailored Using Biomass-Converted Graded Carbon Quantum Dots. *Nanoscale* **2019**, *11*, 15083−15090.
(15) Gu, S.; Hsieh, C.-T.; Ashraf Gandomi, Y.; Li, J.; Yue, X. X.; Chang, J.-K. Tailoring Fluorescence Emissions, Quantum Yields, and White Light Emitting from Nitrogen-Doped Graphene and Carbon Nitride Quantum Dots. *Nanoscale* **2019**, *11*, 16553−16561.
(16) Kou, X.; Jiang, S.; Park, S.-J.; Meng, L.-Y. A Review: Recent Advances in Preparations and Applications of Heteroatom-Doped Carbon Quantum Dots. *Dalton Trans.* **2020**, *49*, 6915−6938.
(17) Sun, Y.-P.; Zhou, B.; Lin, Y.; Wang, W.; Fernando, K. A. S.; Pathak, P.; Meziani, M. J.; Harruff, B. A.; Wang, X.; Wang, H.; Luo, P. G.; Yang, H.; Kose, M. E.; Chen, B.; Veca, L. M.; Xie, S.-Y. Quantum-Sized Carbon Dots for Bright and Colorful Photoluminescence. *J. Am. Chem. Soc.* **2006**, *128*, 7756−7757.
(18) Huang, S.; Li, W.; Han, P.; Zhou, X.; Cheng, J.; Wen, H.; Xue, W. Carbon Quantum Dots: Synthesis, Properties, and Sensing Applications as a Potential Clinical Analytical Method. *Anal. Methods* **2019**, *11*, 2240−2258.
(19) Wang, X.; Feng, Y.; Dong, P.; Huang, J. A Mini Review on Carbon Quantum Dots: Preparation, Properties, and Electrocatalytic Application. *Front. Chem.* **2019**, *7*, 671.
(20) Pan, D.; Zhang, J.; Li, Z.; Wu, M. Hydrothermal Route for Cutting Graphene Sheets into Blue-Luminescent Graphene Quantum Dots. *Adv. Mater.* **2010**, *22*, 734−738.
(21) Guo, X.; Wang, C.-F.; Yu, Z.-Y.; Chen, L.; Chen, S. Facile Access to Versatile Fluorescent Carbon Dots Toward Light-Emitting Diodes. *Chem. Commun.* **2012**, *48*, 2692−2694.
(22) Li, Y.; Hu, Y.; Zhao, Y.; Shi, G.; Deng, L.; Hou, Y.; Qu, L. An Electrochemical Avenue to Green-Luminescent Graphene Quantum Dots as Potential Electron-Acceptors for Photovoltaics. *Adv. Mater.* **2011**, *23*, 776−780.
(23) Hagiwara, K.; Horikoshi, S.; Serpone, N. Photoluminescent Carbon Quantum Dots: Synthetic Approaches and Photophysical Properties. *Chem.—Eur. J.* **2021**, *27*, 9466−9481.
(24) Kim, H. H.; Lee, Y. J.; Park, C.; Yu, S.; Won, S. O.; Seo, W.-S.; Park, C.; Choi, W. K. Bottom-Up Synthesis of Carbon Quantum Dots with High Performance Photo- and Electroluminescence. *Part. Part. Syst. Char.* **2018**, *35*, 1800080.
(25) Shen, T.; Wang, Q.; Guo, Z.; Kuang, J.; Cao, W. Hydrothermal Synthesis of Carbon Quantum Dots Using Different Precursors and Their Combination with TiO_2 for Enhanced Photocatalytic Activity. *Ceram. Int.* **2018**, *44*, 11828−11834.
(26) Xu, Q.; Tang, Y.; Zhu, P.; Zhang, W.; Zhang, Y.; Solis, O. S.; Hu, T. S.; Wang, J. Machine Learning Guided Microwave-Assisted Quantum Dot Synthesis and an Indication of Residual H_2O_2 in Human Teeth. *Nanoscale* **2022**, *14*, 13771−13778.
(27) Ye, R.; Xiang, C.; Lin, J.; Peng, Z.; Huang, K.; Yan, Z.; Cook, N. P.; Samuel, E. L. G.; Hwang, C.-C.; Ruan, G.; Ceriotti, G.; Raji, A.-R. O.; Marti, A. A.; Tour, J. M. Coal as an Abundant Source of Graphene Quantum Dots. *Nat. Commun.* **2013**, *4*, 2943.
(28) Nilewski, L.; Mendoza, K.; Jalilov, A. S.; Berka, V.; Wu, G.; Sikkema, W. K. A.; Metzger, A.; Ye, R.; Zhang, R.; Luong, D. X.; et al. Highly Oxidized Graphene Quantum Dots from Coal as Efficient Antioxidants. *ACS Appl. Mater. Interfaces* **2019**, *11*, 16815−16821.
(29) Das, T.; Saikia, B. K.; Dekaboruah, H. P.; Bordoloi, M.; Neog, D.; Bora, J. J.; Lahkar, J.; Narzary, B.; Roy, S.; Ramaiah, D. Blue-Fluorescent and Biocompatible Carbon Dots Derived from Abundant Low-Quality Coals. *J. Photochem. Photobiol. B Biol.* **2019**, *195*, 1−11.

(30) Saikia, M.; Hower, J. C.; Das, T.; Dutta, T.; Saikia, B. K. Feasibility Study of Preparation of Carbon Quantum Dots from Pennsylvania Anthracite and Kentucky Bituminous Coals. *Fuel* **2019**, *243*, 433−440.
(31) Saikia, M.; Das, T.; Dihingia, N.; Fan, X.; Silva, L. F. O.; Saikia, B. K. Formation of Carbon Quantum Dots and Graphene Nanosheets from Different Abundant Carbonaceous Materials. *Diam. Relat. Mater.* **2020**, *106*, 107813.
(32) Das, T.; Saikia, B. K. Nanodiamonds Produced from Low-Grade Indian Coals. *ACS Sustain. Chem. Eng.* **2017**, *5*, 9619−9624.
(33) Boruah, A.; Roy, K.; Thakur, A.; Haldar, S.; Konwar, R.; Saikia, P.; Saikia, B. K. Biocompatible Nanodiamonds Derived from Coal Washery Rejects: Antioxidant, Antiviral, and Phytotoxic Applications. *ACS Omega* **2023**, *8*, 11151−11160.
(34) Boruah, A.; Saikia, B. K. Chemical Fabrication of Efficient Blue-luminescent Carbon Quantum Dots from Coal Washery Rejects (Waste) for Detection of Hg^{2+} and Cr^{6+} Ions in Water. *ChemistrySelect* **2022**, *7*, No. e202104567.
(35) Boruah, A.; Saikia, M.; Das, T.; Goswamee, R. L.; Saikia, B. K. Blue-Emitting Fluorescent Carbon Quantum Dots from Waste Biomass Sources and Their Application in Fluoride Ion Detection in Water. *J. Photochem. Photobiol. B Biol.* **2020**, *209*, 111940.
(36) Saikia, M.; Das, T.; Saikia, B. K. A Novel Rapid Synthesis of Highly Stable Silver Nanoparticle/Carbon Quantum Dot Nanocomposites Derived from Low-Grade Coal Feedstock. *New J. Chem.* **2022**, *46*, 309−321.
(37) Saikia, M.; Singh, A.; Dihingia, A.; Khare, P.; Kalita, J.; Saikia, B. K. Scalable Production, Cell Toxicity Assessment, and Plant Growth Promotion Activities of Carbon Quantum Dots Derived from Low-Quality Coal Feedstock. *Chem. Eng. J.* **2022**, *433*, 133633.
(38) Song, X.; Guo, Q.; Cai, Z.; Qiu, J.; Dong, G. Synthesis of Multi-Color Fluorescent Carbon Quantum Dots and Solid State Cqds@SiO_2 Nanophosphors for Light-Emitting Devices. *Ceram. Int.* **2019**, *45*, 17387−17394.
(39) Sun, M.; Han, Y.; Yuan, X.; Jing, P.; Zhang, L.; Zhao, J.; Zheng, Y. Efficient Full-Color Emitting Carbon-Dot-Based Composite Phosphors by Chemical Dispersion. *Nanoscale* **2020**, *12*, 15823−15831.
(40) Wang, M.; Han, Y.; Guo, Z.; Huang, Z.; Yang, W. N-Doped Carbon Dots Embedded in Silica Nanoparticles with Multicolor Luminescence for Light-Emitting Devices. *ACS Appl. Nano Mater.* **2021**, *4*, 13625−13632.
(41) Sun, X.; Bruckner, C.; Lei, Y. One-Pot and Ultrafast Synthesis of Nitrogen and Phosphorus Co-Doped Carbon Dots Possessing Bright Dual Wavelength Fluorescence Emission. *Nanoscale* **2015**, *7*, 17278−17282.
(42) Savintsev, A. P.; Gavasheli, Y. O.; Kalazhokov, Z. K.; Kalazhokov, K. K. X-Ray Photoelectron Spectroscopy Studies of the Sodium Chloride Surface After Laser Exposure. *J. Phys.: Conf. Ser.* **2016**, *774*, 012118.
(43) Sarkar, S.; Sudolska, M.; Dubecky, M.; Reckmeier, C. J.; Rogach, A. L.; Zboril, R.; Otyepka, M. Graphitic Nitrogen Doping in Carbon Dots Causes Red-Shifted Absorption. *J. Phys. Chem. C* **2016**, *120*, 1303−1308.
(44) Danks, A. E.; Hall, S. R.; Schnepp, Z. The Evolution of 'Sol−Gel' Chemistry as a Technique for Materials Synthesis. *Mater. Horiz.* **2016**, *3*, 91−112.
(45) Thanh, N. T.; Maclean, N.; Mahiddine, S. Mechanisms of Nucleation and Growth of Nanoparticles in Solution. *Chem. Rev.* **2014**, *114*, 7610−7630.
(46) Larichev, Y. V.; Vodyankina, O. V. Aggregation Mechanisms of Silica Particles in the Sol−Gel Synthesis of Promoted Silver Catalysts. *Kinet. Catal.* **2019**, *60*, 490−495.
(47) Fathy, M.; Abdel Moghny, T.; Mousa, M. A.; El-Bellihi, A.-H. A.-A.; Awadallah, A. E. Absorption of Calcium Ions on Oxidized Graphene Sheets and Study its Dynamic Behavior by Kinetic and Isothermal Models. *Appl. Nanosci.* **2016**, *6*, 1105−1117.
(48) Gui-Long, X.; Changyun, D.; Yun, L.; Pi-Hui, P.; Jian, H.; Zhuoru, Y. Preparation and Characterization of Raspberry-Like SiO_2 Particles by the Sol-Gel Method. *Nanomater. Nanotechnol.* **2011**, *1*, 21.
(49) Yoo, J.; Han, S.; Park, W.; Lee, T.; Park, Y.; Chang, H.; Hahn, S. K.; Kwon, W. Defect-Induced Fluorescence of Silica Nanoparticles for Bioimaging Applications. *ACS Appl. Mater. Interfaces* **2018**, *10*, 44247−44256.
(50) Wang, Y.; Tian, M.; Xie, W.; Li, C. M.; Liu, Y. One-Step Synthesis of Amine-Functionalized Fluorescent Silicon Nanoparticles for Copper (II) Ion Detection. *Anal. Bioanal. Chem.* **2019**, *411*, 6419−6426.

https://doi.org/10.1021/acsomega.3c02884
ACS Omega 2023, 8, 25410−25423